

Supporting Information

Face-on orientation of fluorinated polymers conveyed by long alkyl chains: a prerequisite for high photovoltaic performances

*Olzhas A. Ibraikulov, Chheng Ngo, Patricia Chávez, Ibrahim Bulut, Benoît Heinrich, Olivier Boyron, Kirill L. Gerasimov, Dimitri A. Ivanov, Sufal Swaraj, Stéphane Méry, Nicolas Leclerc, * Patrick Lévêque* and Thomas Heiser**

Table of Content:

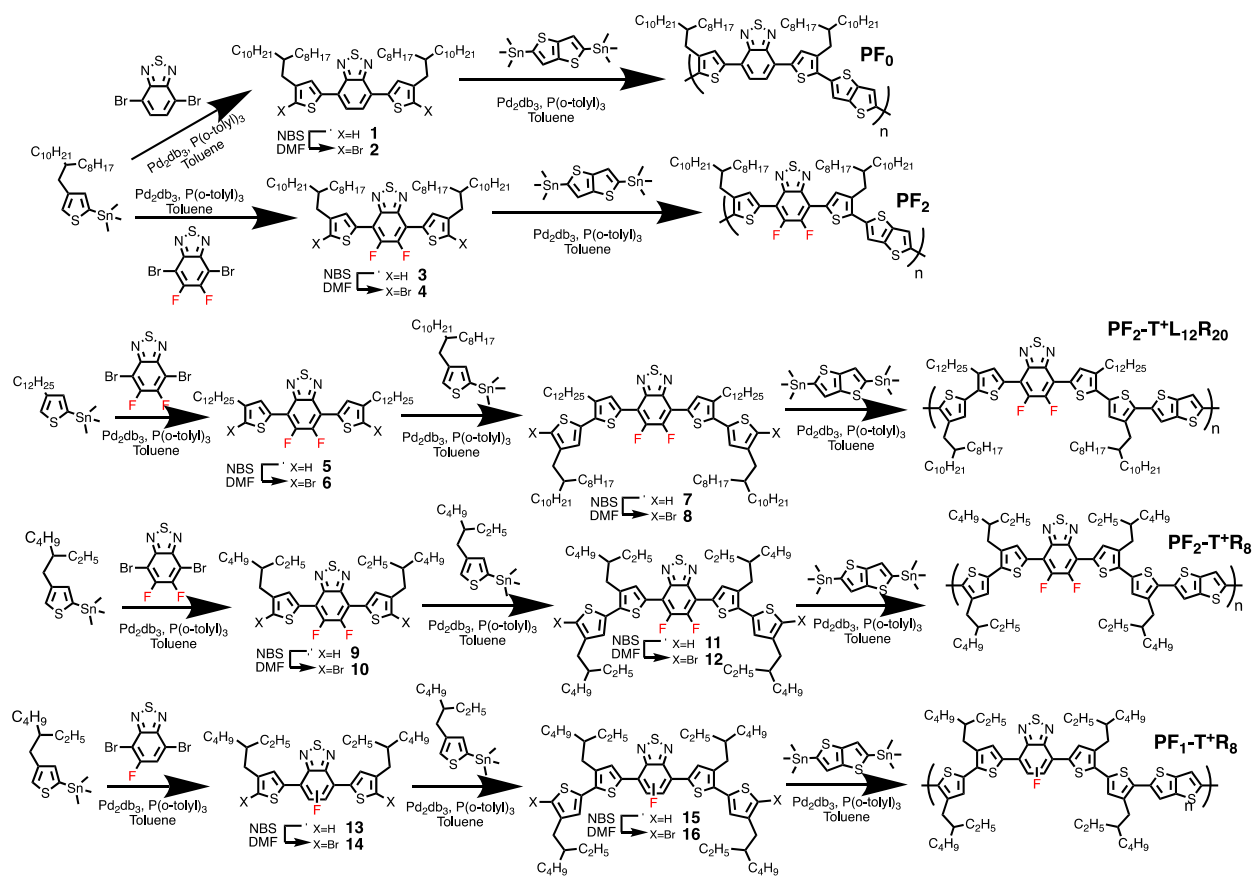
1	Materials: Synthesis and molecular characterizations	p. 2
2	Electrochemical measurements	p. 11
3	UV-visible measurements	P. 12
4	Thermal properties	P. 13
5	Grazing Incidence Wide Angle X-ray Scattering measurements (GIWAXS)	
	P. 14	
6	Scanning Transmission X-ray Microscopy characterizations (STXM)	
	P.19	
7	Fabrication and characterization of solar cells	P. 19
8	Transient photovoltage and charge extraction measurements	P. 20
9	OFET and SCLC devices	p. 24

1 Materials: Synthesis and molecular characterizations.

All reagents and chemicals were purchased from Aldrich and TCI. Toluene (ACS grade) was distilled from Na/benzophenone. The synthesis of the 2-(trimethylstannyl)-4-(2-octyldodecyl)thiophene, 2-(trimethylstannyl)-4-(dodecyl)thiophene, 2-(trimethylstannyl)-4-(2-ethylhexyl)thiophene and 2-5-bis-trimethylstannyl-thieno[3,2-*b*]thiophene have been prepared as described in the literature.^[1]

NMR analysis. ¹H and ¹³C NMR spectra were recorded on a Bruker 400 Ultrashield™ 400 MHz NMR spectrometer, with an internal lock on the ²H-signal of the solvent (CDCl₃).

Size exclusion chromatography. Size Exclusion Chromatography (SEC) measurements were performed with a Waters Alliance GPCV 2000 instrument (Milford/MA) that incorporates a differential refractive index and a viscosimeter. 1,2,4-Trichlorobenzene was used as the mobile phase at a flow rate of 1 mL/min at 150°C. It was stabilized with 2,6-di(*tert*-butyl)-4-methylphenol. The polymer was injected at a concentration of 1 mg/mL. The separation was carried out on three Agilent columns (PL gel Olexis 7*300 mm) protected by a guard column (PL gel 5 μm). Columns and detectors were maintained at 150°C. The Empower software was used for data acquisition and analysis. The molar mass distributions were calculated with a calibration curve based on narrow polystyrene standards (Polymer Standard Service, Mainz), using only the refractometer detector.



Scheme S1: Synthetic routes of reported polymers in this work

General procedure for Stille cross-coupling.

A flame dried Schlenk was charged with the dibromo-compound (1.0 equiv.) and the 2-(trimethylstannyl)-4-(alkyl)thiophene compound (2.2 equiv.). Anhydrous and degassed toluene (0.1M) was added under inert gas. Finally, the $\text{Pd}_2(\text{dba})_3$ (2.0 mol%) and $\text{P}(o\text{-tolyl})_3$ (8.0 mol%) were added in one portion and the mixture was stirred 24 hours at 120°C. After cooling to room temperature the reaction mixture was filtered through a pad of celite and the toluene solution was evaporated under reduced pressure. Then, the crude material was purified by column chromatography.

4,7-bis(4-(2-octyldodecyl)thiophen-2-yl)benzo[*c*][1,2,5]thiadiazole (compound 1).

The crude product was purified by column chromatography (silica gel, petroleum ether).

Yield: 72%.

^1H NMR (400 MHz, CDCl_3) δ (ppm) = 7.94 (d, $^4J= 1.1$ Hz, 2H), 7.82 (s, 2H), 7.00 (d, $^4J= 0.7$ Hz, 2H), 2.62 (d, $^3J= 6.7$ Hz, 4H), 1.69 (m, 2H), 1.24 (m, 64H), 0.86 (t, $^3J= 6.02$ Hz, 12H).

^{13}C NMR (100 MHz, CDCl_3) δ (ppm) = 152.7, 143.0, 138.8, 129.5, 126.0, 125.5, 122.4, 38.9, 35.1, 33.3, 31.9, 30.0, 29.71, 29.68, 29.4, 26.6, 22.7, 14.1.

5,6-difluoro-4,7-bis(4-(2-octyldodecyl)thiophen-2-yl)benzo[*c*][1,2,5]thiadiazole (compound 3).

The crude product was purified by column chromatography (silica gel, petroleum ether). Yield: 65%.

^1H NMR (400 MHz, CDCl_3) δ (ppm) = 8.09 (d, $^4J= 1.1$ Hz, 2H), 7.17 (d, $^4J= 1.0$ Hz, 2H), 2.65 (d, $^3J= 6.7$ Hz, 4H), 1.70 (m, 2H), 1.26 (m, 64H), 0.87 (t, $^3J= 6.0$ Hz, 12H).

^{13}C NMR (100 MHz, CDCl_3) δ (ppm) = 151.4 (dd, $J= 256.5$ and 20.4 Hz), 149.0 (t, $J= 4.23$ Hz), 142.37, 132.9 (d, $J=3.8$ Hz), 131.0, 124.81, 111.69 (dd, $J=9.1$ and 4.9 Hz), 39.0, 34.9, 33.4, 31.9, 30.0, 29.7, 29.6, 29.3, 26.7, 22.6, 14.0.

5,6-difluoro-4,7-bis(4-(dodecyl)thiophen-2-yl)benzo[*c*][1,2,5]thiadiazole (compound 5).

The crude product was purified by column chromatography (silica gel, petroleum ether/methylene chloride: 5/1). Yield: 73%.

^1H NMR (400 MHz, Toluene d_8) δ (ppm) = 8.34 (d, $^4J= 1.3$ Hz, 2H), 6.90 (d, $^4J= 1.3$ Hz, 2H), 2.62 (d, $^3J= 6.7$ Hz, 4H), 1.68 (m, 4H), 1.38 (m, 36H), 0.96 (t, $^3J= 6.5$ Hz, 6H).

Because of a poor solubility, any ^{13}C NMR spectrum has been recorded for this compound.

4,7-bis(3-dodecyl-4'-(2-octyldodecyl)-[2,2'-bithiophen]-5-yl)-5,6-difluorobenzo[*c*][1,2,5]thiadiazole (compound 7).

The crude product was purified by column chromatography (silica gel, petroleum ether/methylene chloride: 95/5). Yield: 70%.

^1H NMR (400 MHz, CDCl_3) δ (ppm) = 8.12 (s, 2H), 7.07 (d, $^4J= 1.1$ Hz, 2H), 6.93 (d, $^4J= 0.7$ Hz, 2H), 2.86 (t, $^3J= 7.3$ Hz, 4H), 2.57 (d, $^3J= 6.7$ Hz, 4H), 1.72 (m, 8H), 1.27 (m, 98H), 0.88 (t, $^3J= 6.90$ Hz, 18H).

^{13}C NMR (100 MHz, CDCl_3) δ (ppm) = 151.5 (dd, J = 259.4 and 19.2 Hz), 148.8 (t, J = 4.1 Hz), 142.6, 139.5, 135.2, 135.0, 134.0 (d, J = 4.5 Hz), 129.0, 128.2, 121.6, 38.9, 35.0, 33.4, 31.9, 30.6, 30.1, 29.72, 29.68, 29.6, 29.5, 29.4, 26.7, 22.7, 14.1.

4,7-bis(4-(2-ethylhexyl)thiophen-2-yl)-5,6-difluorobenzo[*c*][1,2,5]thiadiazole (compound 9).

The crude product was purified by column chromatography (silica gel, petroleum ether/methylene chloride: 9/1). Yield: 89%.

^1H NMR (400 MHz, CDCl_3) δ (ppm) = 8.05 (d, 4J = 0.9 Hz, 2H), 7.17 (d, 4J = 0.9 Hz, 2H), 2.65 (d, 3J = 6.9 Hz, 4H), 1.65 (m, 2H), 1.32 (m, 16H), 0.92 (t, 3J = 6.9 Hz, 12H).

^{13}C NMR (100 MHz, CDCl_3) δ (ppm) = 152.9 (dd, J = 256.7 and 19.8 Hz), 148.9 (t, J = 4.34 Hz), 142.4, 132.8, 131.0, 124.8 (t, J = 2.99 Hz), 111.7 (dd, J = 3.8 and 12.5 Hz), 40.4, 34.5, 32.5, 28.9, 25.7, 23.0, 14.1, 10.9.

4,7-bis(3,4'-bis(2-ethylhexyl)-[2,2'-bithiophen]-5-yl)-5,6-difluorobenzo[*c*][1,2,5]thiadiazole (compound 11).

The crude product was purified by column chromatography (silica gel, petroleum ether/methylene chloride: 9/1). Yield: 97%.

^1H NMR (400 MHz, CDCl_3) δ (ppm) = 8.06 (s, 2H), 7.07 (d, 4J = 0.9 Hz, 2H), 6.92 (d, 4J = 0.9 Hz, 2H), 2.78 (d, 3J = 7.3 Hz, 4H), 2.56 (d, 3J = 6.9 Hz, 4H), 1.74 (m, 2H), 1.60 (m, 2H), 1.30 (m, 32H), 0.90 (m, 24H).

^{13}C NMR (100 MHz, CDCl_3) δ (ppm) = 151.5 (dd, J = 259.7 and 18.7 Hz), 148.9 (t, J = 4.6 Hz), 142.5, 138.8, 135.7 (t, J = 3.6 Hz), 135.1, 134.6 (t, J = 4.3 Hz), 129.0, 128.5, 121.6, 111.2 (dd, J = 4.6 and 8.5 Hz), 40.4, 40.2, 34.6, 33.5, 32.6, 28.9, 28.7, 25.8, 25.7, 23.1, 23.0, 14.1, 14.0, 10.9, 10.7.

4,7-bis(4-(2-ethylhexyl)thiophen-2-yl)-5-fluorobenzo[*c*][1,2,5]thiadiazole (compound 13).

The crude product was purified by column chromatography (silica gel, petroleum ether). Yield: 92%.

^1H NMR (400 MHz, CDCl_3) δ (ppm) = 8.04 (s, 1H), 7.93 (d, $^4J = 1.3$ Hz, 1H), 7.71 (d, $J_{H-F} = 13.0$ Hz, 1H), 7.11 (d, $^4J = 1.0$ Hz, 1H), 7.04 (s, 1H), 2.62, (t, $^3J = 5.3$ Hz, 4H), 1.63 (m, 2H), 1.29 (m, 16H), 0.88 (m, 12H).

^{13}C NMR (100 MHz, CDCl_3) δ (ppm) = 159.0 (d, $J = 253.7$ Hz), 153.5 (d, $J = 11.2$ Hz), 149.8, 143.2, 142.2, 137.4 (d, $J = 2.51$ Hz), 132.0 (d, $J = 8.4$ Hz), 131.9, 130.3, 125.8 (d, $J = 11.1$ Hz), 123.8 (d, $J = 6.9$ Hz), 123.6, 116.7 (d, $J = 32.4$ Hz), 111.2 (d, $J = 15.3$ Hz), 40.4, 40.3, 34.6, 34.5, 32.5, 28.5, 28.9, 25.6, 23.1, 23.08, 14.2, 10.9, 10.87.

4,7-bis(3,4'-bis(2-ethylhexyl)-[2,2'-bithiophen]-5-yl)-5-fluorobenzo[*c*][1,2,5]thiadiazole (compound 15).

The crude product was purified by column chromatography (silica gel, petroleum ether). Yield: 86%.

^1H NMR (400 MHz, CDCl_3) δ (ppm) = 8.08 (s, 1H), 7.95 (s, 1H), 7.72 (d, $J_{H-F} = 13.1$ Hz, 1H), 7.07 (t, $^4J = 1.6$ Hz, 2H), 6.92 (dd, $^4J = 1.2$ and 2.97 Hz, 2H), 2.81 (d, $^3J = 5.4$ Hz, 2H), 2.79 (d, $^3J = 5.4$ Hz, 2H), 2.57 (d, $^3J = 6.8$ Hz, 4H), 1.75 (m, 2H), 1.61 (m, 2H), 1.31 (m, 32H), 0.89 (m, 12H).

^{13}C NMR (100 MHz, CDCl_3) δ (ppm) = 160.7, 157.3, 153.5 (d, $J = 11.4$ Hz), 149.8, 142.5, 142.3, 139.5, 138.7, 135.1 (t, $J = 1.2$ Hz), 134.6 (t, $J = 1.5$ Hz), 133.8 (d, $J = 6.2$ Hz), 133.7, 131.9, 130.1, 130.0, 128.4 (d, $J = 10.9$ Hz), 125.4, 125.2, 121.4 (d, $J = 15.5$ Hz), 111.0, 110.8, 40.4, 40.2, 34.62, 34.6, 33.6, 33.5, 32.6, 28.9, 28.7, 25.8, 25.7, 23.1, 23.0, 14.1, 10.9, 10.7.

General procedure for di-bromination.

The initial conjugated compound, as obtained after Stille cross-coupling, (1.0 equiv.) was solubilized in DMF (0.05 M) under argon in the dark. NBS (2.0 equiv.) was added portion wise. The resulting solution was stirred at room temperature under argon overnight. Water and diethylether were added and the resulting solution was stirred for 2h. The organic phase was separated from the water phase and extracted with brine (3 x 100 mL). The organic phase

was dried with sodium sulfate, filtered and the solvent evaporated under reduced pressure. The crude product was purified by column chromatography.

4,7-bis(5-bromo-4-(2-octyldodecyl)thiophen-2-yl)benzo[*c*][1,2,5]thiadiazole (compound 2).

The crude product was purified by column chromatography (silica gel, petroleum ether). Yield: 72%.

¹H NMR (400 MHz, CDCl₃) δ (ppm) = 7.76 (s, 2H), 7.75 (s, 2H), 2.58 (d, ³*J*= 7.1 Hz, 4H), 1.76 (m, 2H), 1.25 (m, 64H), 0.87 (t, ³*J*= 5.4 Hz, 12H).

¹³C NMR (100 MHz, CDCl₃) δ (ppm) = 152.3, 142.3, 138.3, 128.7, 125.3, 124.9, 112.2, 38.6, 34.3, 33.4, 31.9, 30.0, 29.7, 29.67, 29.65, 29.4, 26.6, 22.7, 14.1.

4,7-bis(5-bromo-4-(2-octyldodecyl)thiophen-2-yl)-5,6-difluorobenzo[*c*][1,2,5]thiadiazole (compound 4)

The crude product was purified by column chromatography (silica gel, petroleum ether). Yield: 78%.

¹H NMR (400 MHz, CDCl₃) δ (ppm) = 7.90 (s, 2H), 2.57 (d, ³*J*= 7.0 Hz, 4H), 1.74 (m, 2H), 1.25 (m, 64H), 0.86 (t, ³*J*= 5.4 Hz, 12H).

¹³C NMR (100 MHz, CDCl₃) δ (ppm) = 152.4 (dd, *J*= 260.3 and 20.4 Hz), 148.4 (t, *J*= 4.2 Hz), 141.8, 132.3 (t, *J*= 4.7 Hz), 131.0, 115.1 (t, *J*= 3.6 Hz), 111.0 (dd, *J*= 4.7 and 13.3 Hz), 38.6, 34.2, 33.4, 31.9, 30.0, 29.7, 29.65, 29.61, 29.3, 26.6, 22.7, 14.1.

4,7-bis(5-bromo-4-dodecylthiophen-2-yl)-5,6-difluorobenzo[*c*][1,2,5]thiadiazole (compound 6).

Because of a poor solubility, this compound has been used without purification by column chromatography.

¹H NMR (400 MHz, Toluene d₈) δ (ppm) = 7.85 (s, 2H), 2.62 (d, ³*J*= 6.7 Hz, 4H), 1.68 (m, 4H), 1.38 (m, 36H), 0.96 (t, ³*J*= 6.5 Hz, 6H).

Because of a poor solubility, any ¹³C NMR spectrum has been recorded for this compound.

4,7-bis(5'-bromo-4'-(2-decyldodecyl)-3-dodecyl-[2,2'-bithiophen]-5-yl)-5,6-difluorobenzo[c][1,2,5]thiadiazole (compound 8).

The crude product was purified by column chromatography (silica gel, petroleum ether).

Yield: 89%.

^1H NMR (400 MHz, CDCl_3) δ (ppm) = 8.10 (s, 2H), 6.92 (s, 2H), 2.81 (t, $^3J= 7.3$ Hz, 4H), 2.52 (d, $^3J= 6.6$ Hz, 4H), 1.72 (m, 8H), 1.27 (m, 98H), 0.88 (t, $^3J= 6.9$ Hz, 18H).

^{13}C NMR (100 MHz, CDCl_3) δ (ppm) = 151.0 (dd, $J= 261.0$ and 20.4 Hz), 148.7 (t, $J= 3.9$ Hz), 141.9, 139.9, 134.9, 134.1 (t, $J= 3.8$ Hz), 133.9 (t, $J= 4.1$ Hz), 129.5, 127.6, 111.1 (dd, $J= 3.9$ and 10.2 Hz), 110.0, 38.6, 34.2, 33.4, 31.9, 30.6, 30.1, 29.73, 29.70, 29.6, 29.5, 29.4, 26.6, 22.7, 14.1.

4,7-bis(5-bromo-4-(2-ethylhexyl)thiophen-2-yl)-5,6-difluorobenzo[c][1,2,5]thiadiazole (compound 10).

The crude product was purified by column chromatography (silica gel, petroleum ether).

Yield: 79%.

^1H NMR (400 MHz, CDCl_3) δ (ppm) = 7.91 (s, 2H), 2.58 (d, $^3J= 7.2$ Hz, 4H), 1.69 (m, 2H), 1.32 (m, 16H), 0.92 (t, $^3J= 7.1$ Hz, 12H).

^{13}C NMR (100 MHz, CDCl_3) δ (ppm) = 160.2, 151.6 (dd, $J= 257.6$ and 18.2 Hz), 148.5, 144.8, 132.3 (t, $J= 4.82$ Hz), 131.1, 115.1 (t, $J= 4.22$ Hz), 111.1 (dd, $J= 6.4$ and 14.1 Hz), 40.0, 33.8, 32.5, 28.8, 25.6, 23.0, 14.1, 10.8.

4,7-bis(5'-bromo-3,4'-bis(2-ethylhexyl)-[2,2'-bithiophen]-5-yl)-5,6-difluorobenzo[c][1,2,5]thiadiazole (compound 12).

The crude product was purified by column chromatography (silica gel, petroleum ether).

Yield: 77%.

^1H NMR (400 MHz, CDCl_3) δ (ppm) = 8.05 (s, 2H), 6.91 (s, 2H), 2.75 (d, $^3J= 7.3$ Hz, 4H), 2.51 (d, $^3J= 7.2$ Hz, 4H), 1.68 (m, 4H), 1.31 (m, 32H), 0.88 (m, 24H).

^{13}C NMR (100 MHz, CDCl_3) δ (ppm) = 151.1 (dd, J = 260.1 and 20.4 Hz), 148.7 (t, J = 3.9 Hz), 144.8, 139.2, 134.9, 134.6 (t, J = 3.6 Hz), 134.5 (t, J = 4.5 Hz), 129.4, 127.9, 111.1 (dd, J = 3.6 and 9.3 Hz), 110.1, 40.2, 40.0, 33.8, 33.5, 32.6, 32.5, 28.8, 28.7, 25.7, 23.12, 23.10, 14.2, 10.9, 10.7.

4,7-bis(5-bromo-4-(2-ethylhexyl)thiophen-2-yl)-5-fluorobenzo[*c*][1,2,5]thiadiazole (compound 14).

The crude product was purified by column chromatography (silica gel, petroleum ether).
Yield: 93%.

^1H NMR (400 MHz, CDCl_3) δ (ppm) = 7.92 (s, 1H), 7.72 (s, 1H), 7.63 (d, J_{H-F} = 13.0 Hz, 1H), 2.55 (t, 3J = 5.7 Hz, 4H), 1.70 (m, 2H), 1.33 (m, 16H), 0.94 (t, 3J = 7.3 Hz, 12H).

^{13}C NMR (100 MHz, CDCl_3) δ (ppm) = 160.2, 157.7, 153.0 (d, J = 10.8 Hz), 149.4, 142.4, 141.5, 136.9 (d, J = 2.8 Hz), 132.1 (d, J = 5.6 Hz), 131.6 (d, J = 9.5 Hz), 120.34, 125.0 (d, J = 11.3 Hz), 116.0 (d, J = 32.4 Hz), 113.8 (dd, J =9.5 and 4.8 Hz), 110.7 (d, J =14.9 Hz), 40.2, 40.0, 33.9, 33.8, 32.5, 28.8, 25.8, 23.0, 14.1, 10.8.

4,7-bis(5'-bromo-3,4'-bis(2-ethylhexyl)-[2,2'-bithiophen]-5-yl)-5-fluorobenzo[*c*][1,2,5]thiadiazole (compound 16).

The crude product was purified by column chromatography (silica gel, petroleum ether).
Yield: 87%.

^1H NMR (400 MHz, CDCl_3) δ (ppm) = 8.05 (s, 1H), 7.91 (s, 1H), 7.71 (d, J_{H-F} = 13.1 Hz, 1H), 6.90 (d, 4J = 1.5 Hz, 2H), 2.74 (t, 3J = 5.3 Hz, 4H), 2.52 (t, 3J = 7.2 Hz, 4H), 1.68 (m, 4H), 1.30 (m, 32H), 0.89 (m, 24H).

^{13}C NMR (100 MHz, CDCl_3) δ (ppm) = 160.3, 157.4, 153.5, 149.9, 142.0 (d, J = 5.9 Hz), 140.3, 139.4, 135.7, 135.4 (d, J = 13.5 Hz), 133.9 (d, J = 6.4 Hz), 131.7 (d, J = 7.6 Hz), 132.0, 130.7 (d, J = 5.4 Hz), 128.1 (d, J = 12.24 Hz), 125.5, 125.4, 116.0 (d, J = 32.4 Hz), 113.8 (d, J =19.8 Hz), 110.7 (d, J =20.0 Hz), 40.5, 40.2, 34.1, 33.8, 33.7, 32.8, 29.0, 28.9, 26.0, 25.98, 23.3, 23.2, 14.3, 11.0, 10.9.

General Stille polymerization procedure.

A flame dried Schlenk was charged with dibrominated compound (1.0 equiv) and the 2-5-bis-trimethylstannyl-thieno[3,2-*b*]thiophene (1.0 equiv.). Anhydrous and degassed toluene (0.0125 M) was added under inert gas. Then, the Pd₂(dba)₃ (2 mol%) and P(*o*-tolyl)₃ (8 mol%) were added in one portion and the mixture was stirred 24 hours at 120°C. The reaction was quenched with 2-(trimethylstannyl)-thiophene (0.6 equiv.) during 1 hour followed by 2-bromothiophene (0.6 equiv.). Then, the polymer crude was purified by precipitation in methanol, filtered and separated by Soxhlet extraction with methanol, acetone, cyclohexane and chlorobenzene. Then, the sodium diethyldithiocarbamate solution was added in the chlorobenzene fraction and the mixture was stirred at 60°C during 1 hour. The organic phase was washed with water, separated and evaporated under reduced pressure. Finally, the polymer was precipitated in methanol, filtered and dried under reduced pressure at 40°C overnight, providing powder with a metallic shine.

PF₀ Polymer

M_n = 44 kg/mol, M_w = 62 kg/mol and Đ = 1.4

PF₂ Polymers

Batch 1: M_n = 17 kg/mol, M_w = 44 kg/mol and Đ = 2.6

Batch 2: M_n = 29 kg/mol, M_w = 58 kg/mol and Đ = 2.0

Batch 3: M_n = 35 kg/mol, M_w = 63 kg/mol and Đ = 1.8

Batch 4: M_n = 45 kg/mol, M_w = 103 kg/mol and Đ = 2.3

PF₂-T⁺L₁₂R₂₀ Polymer

M_n = 32 kg/mol, M_w = 69 kg/mol and Đ = 2.1

PF₂-T⁺R₈ Polymer

M_n = 14 kg/mol, M_w = 20 kg/mol and Đ = 1.4

PF₁-T⁺R₈ Polymer

Mn = 27 kg/mol, Mw = 52 kg/mol and Đ = 1.94

Table S1: Optoelectronic and molecular properties of polymers

Polymers	M _n (kg/mol)	Đ	HOMO ^{CV}	LUMO ^{opt}	E _G ^{opt}
PF ₀	44	1.4	5.20	3.62	1.58
PF ₂ (batch 1)	17	2.6	5.42	3.78	1.64
PF ₂ (batch 2)	29	2.0			
PF ₂ (batch 3)	35	1.8			
PF ₂ (batch 4)	45	2.3			
PF ₁ -T ⁺ R ₈	27	1.9	5.31	3.71	1.60
PF ₂ -T ⁺ R ₈	14	1.4	5.44	3.84	1.60
PF ₂ -T ⁺ L ₁₂ R ₂₀	32	2.1	5.58	4.02	1.60

Mn – molecular weight in numbers

Đ – polydispersity index

HOMO^{CV} – HOMO level derived from cyclic voltammetry measurements

LUMO^{opt} – LUMO level calculated using the value of optical band gap

E_G^{opt} – optical band gap

2 Electrochemical measurements.

Oxidation and reduction potentials were determined by cyclic voltammetry with a conventional 3-electrode system using a voltammetric analyzer equipped with a platinum micro disk (2 mm²) working electrode and a platinum wire counter electrode. Potentials were calibrated versus the saturated calomel electrode (SCE) at a conventional scan rate of 100 mV/s. Recrystallized tetrabutylammonium hexafluorophosphate (Bu₄NPF₆) was used as the supporting electrolyte (0.1 M) in distilled and anhydrous acetonitrile. Acetonitrile was distilled from CaH₂ under a nitrogen atmosphere. The ferrocene/ferricenium couple was used as an internal reference.

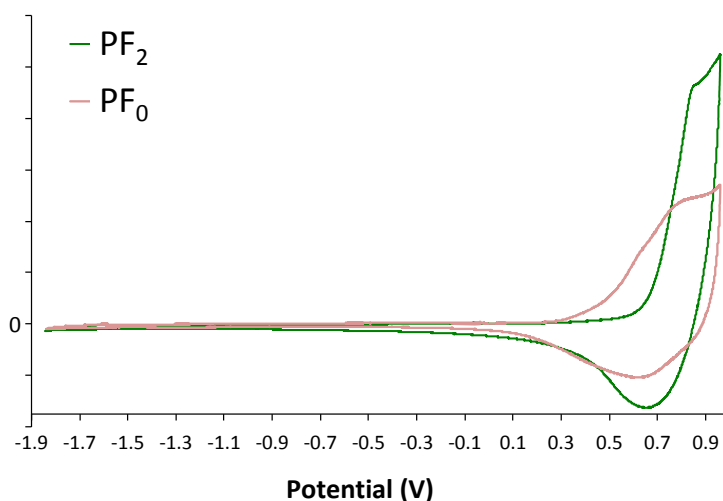


Figure S1: Cyclic voltammetry (CV) curves.

3 UV-visible measurements.

Both in-situ UV-vis temperature dependent experiments in solution and measurements of polymers and blends in thin films were performed using an Agilent Cary Spectrophotometer. For solutions, polymers were dissolved in *o*-DCB solutions at relatively low concentrations (0.01-0.015 mg/mL for both) to ensure transparency. Optical analyzes in thin films were executed on as-deposited samples by spincoating of polymers and blends from *o*-DCB solutions (6-8 mg/mL) at 600 rpm during 180 s under nitrogen ambient on ITO/PEIE pre-coated glass substrates.

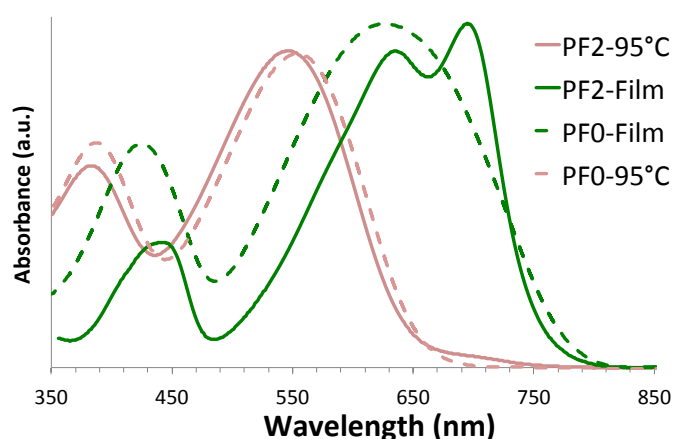


Figure S2: UV-vis absorption spectra in *o*DCB solution at 95°C (pink lines) and in thin-films (green lines) of PF₀ (dashed lines) and PF₂ (full line).

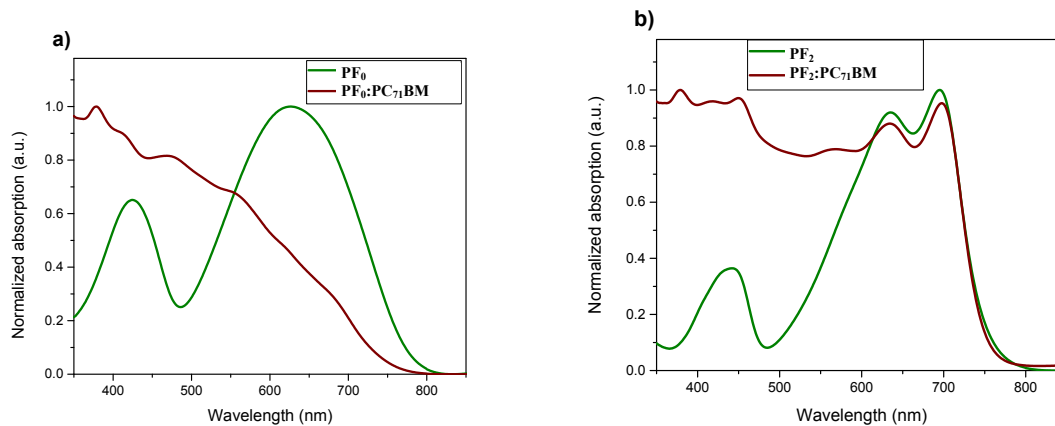
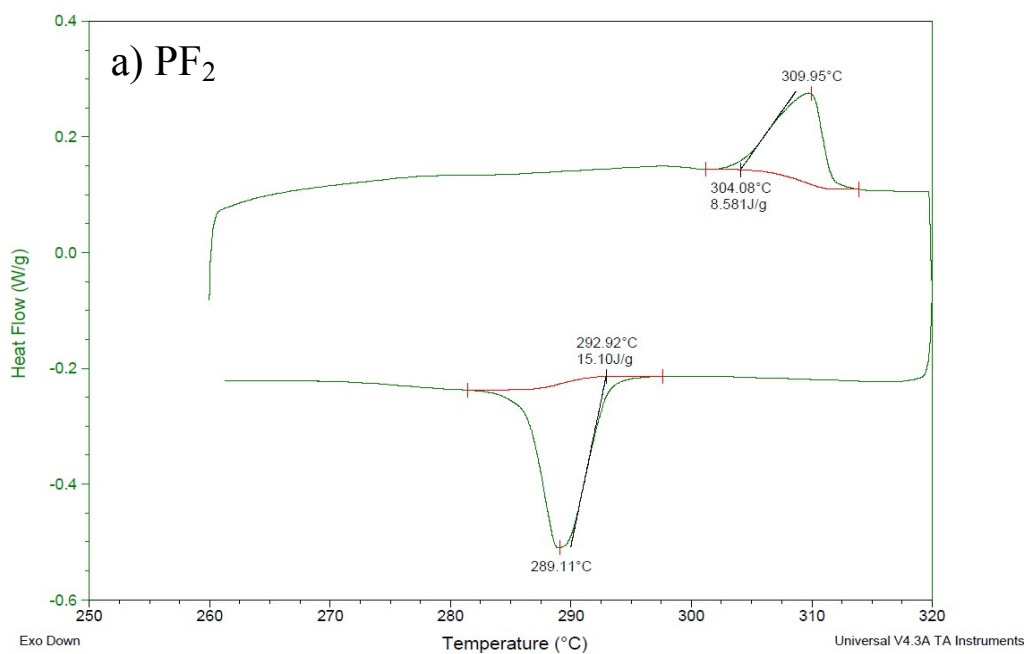


Figure S3: UV-vis spectra of pure **PF₀** and **PF₂** thin films and of **polymer:PC₇₁BM** blends (ratio: 1:1.5).

4 Thermal properties.

DSC measurements were performed with TA Instruments Q1000 instrument, operated at scan rate of 5°C/min on heating and on cooling.



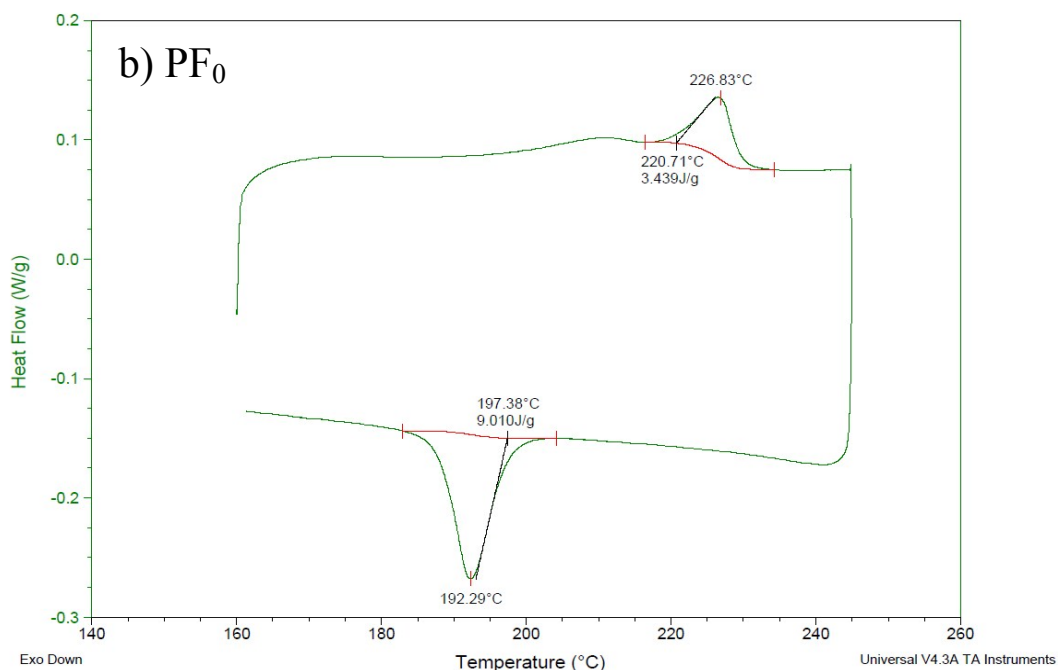


Figure S4: Differential scanning calorimetry (DSC) curves. a) PF₂ and b) PF₀.

5 Grazing Incidence Wide Angle X-ray Scattering measurements (GIWAXS).

GIWAXS measurements were conducted at PLS-II 9A U-SAXS beamline of Pohang Accelerator Laboratory (PAL) in Korea. The X-rays coming from the vacuum undulator (IVU) were monochromated using Si(111) double crystals and focused on the detector using K-B type mirrors. Patterns were recorded with a 2D CCD detector (Rayonix SX165). The sample-to-detector distance was about 225 mm for energy of 11.07 keV (1.200 Å)

GIWAXS measurements were also performed on the ID-10 beamline of the European Synchrotron Radiation Facility (ESFR) in Grenoble (France). Diffraction patterns were collected with a Pilatus 300k detector (172 × 172 μm² pixel size). The wavelength used was 1.24 Å. The measurements were performed on thin films deposited on Si substrate at an incidence angle of 0.16°. The modulus of the scattering vector was calibrated using several diffraction orders of silver behenate. The reduction and integration of 2D-WAXS patterns was performed with home-made routine built in Igor Pro software (Wavemetrics Ltd).

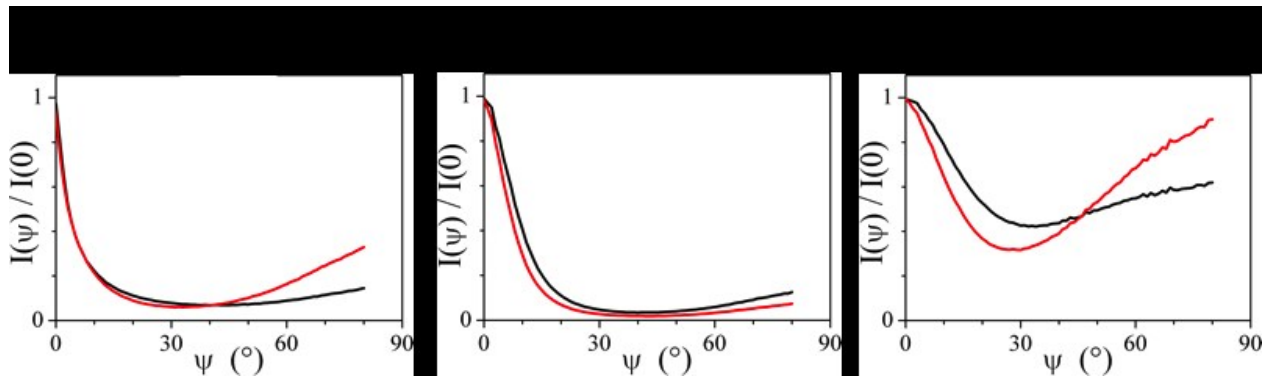
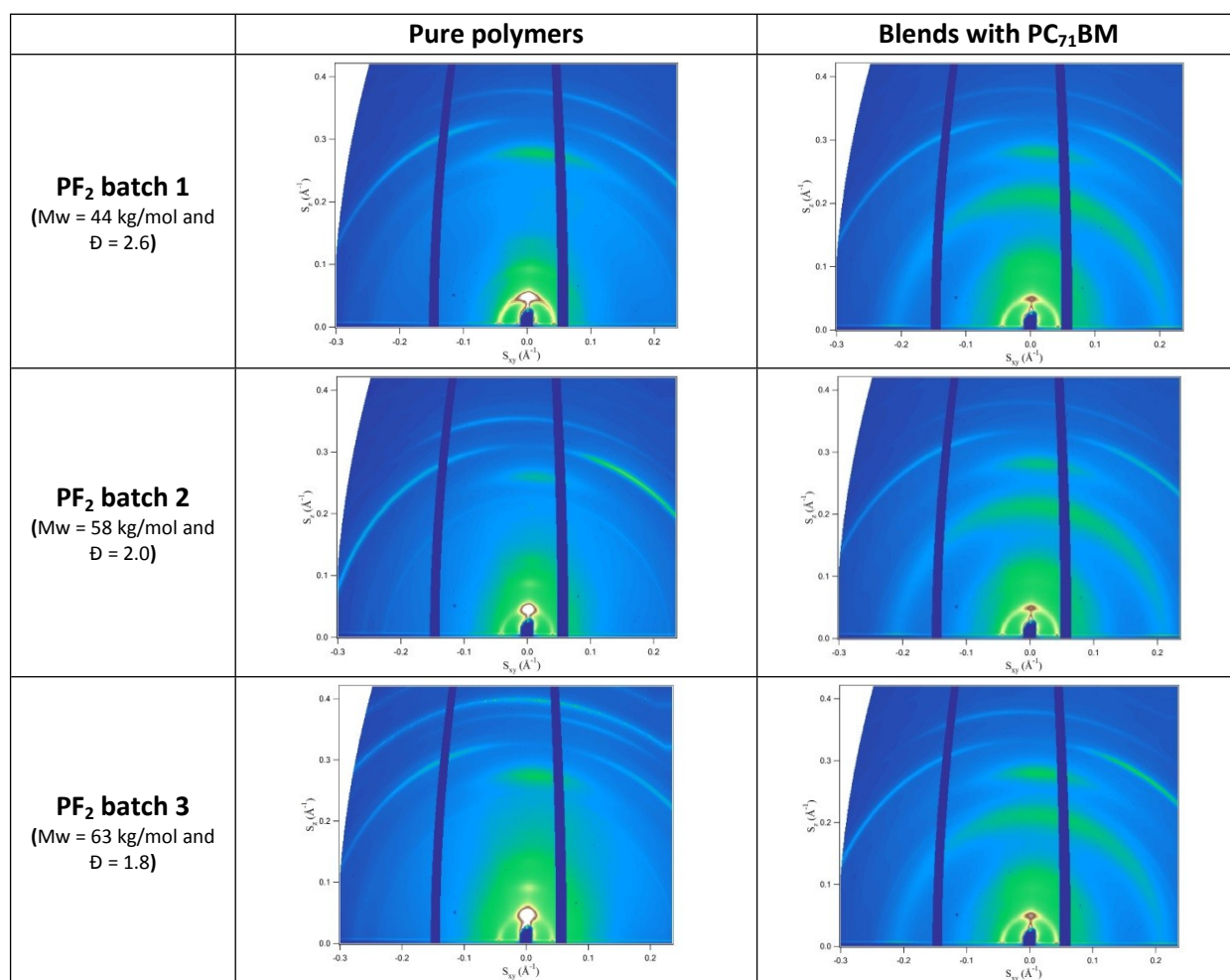


Figure S5: GIWAXS additional curves (radial plots) on PF_0 , PF_2 and $\text{PF}_2\text{-T}^+\text{L}_{12}\text{R}_{20}$ at rotation speed of 600 rpm (black curves) and 2000 rpm (red curves)



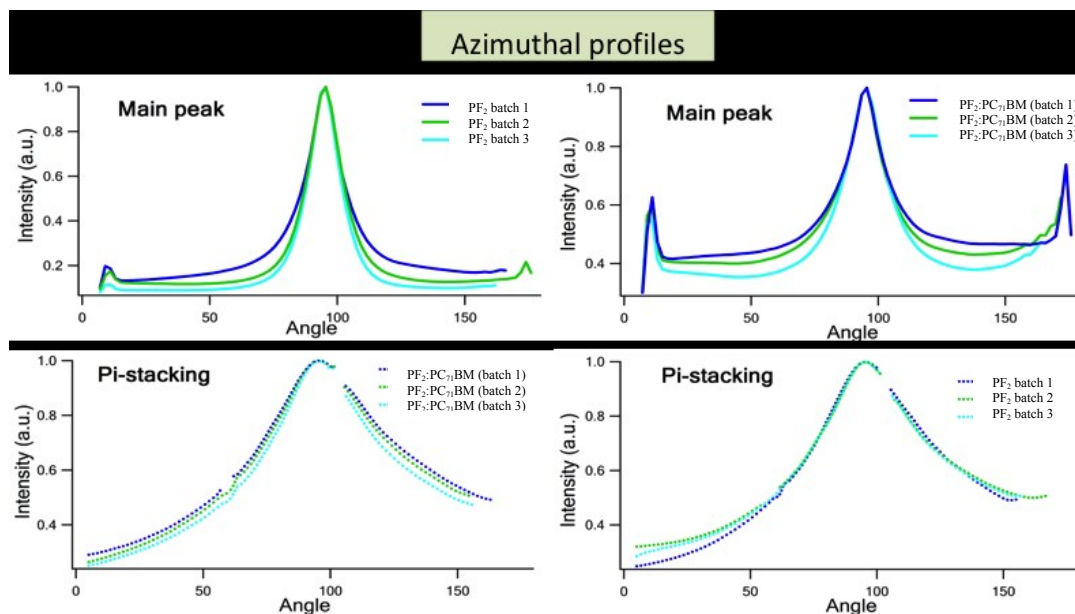


Figure S6. (Top) 2D GIWAXS patterns measured on thin films of **PF₂ batch x** ($x=1-3$) with different molecular weights (left column) and their blends with PC₇₁BM (right column). **(Bottom)** The azimuthal intensity profiles of the 100 peak and π - π stacking peaks.

n.b. GIWAXS measurements performed on PF₂:PC₇₁BM blends with different molar mass (batch 1, 2 or 3) (Figure S6) reveal that the disorder in the lamellar orientation increases with decreasing molar mass and correlates well with the observed decrease in hole mobility for the low molar mass polymer blends (see charge transport section of the Supporting Information).

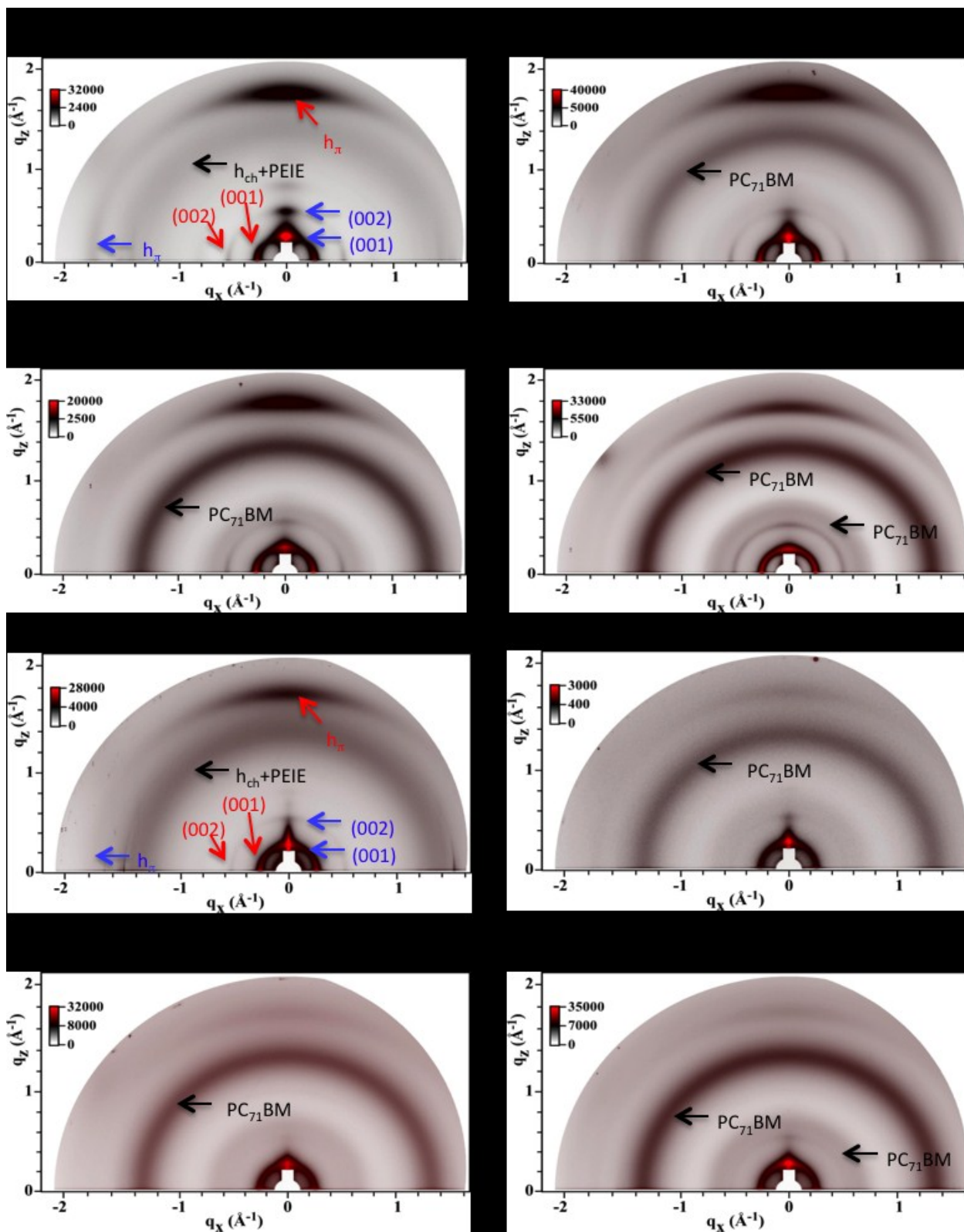


Figure S7: GIWAXS patterns of PF_2 : PC_{71}BM and PF_0 : PC_{71}BM blends with various polymer:fullerene weight ratios.

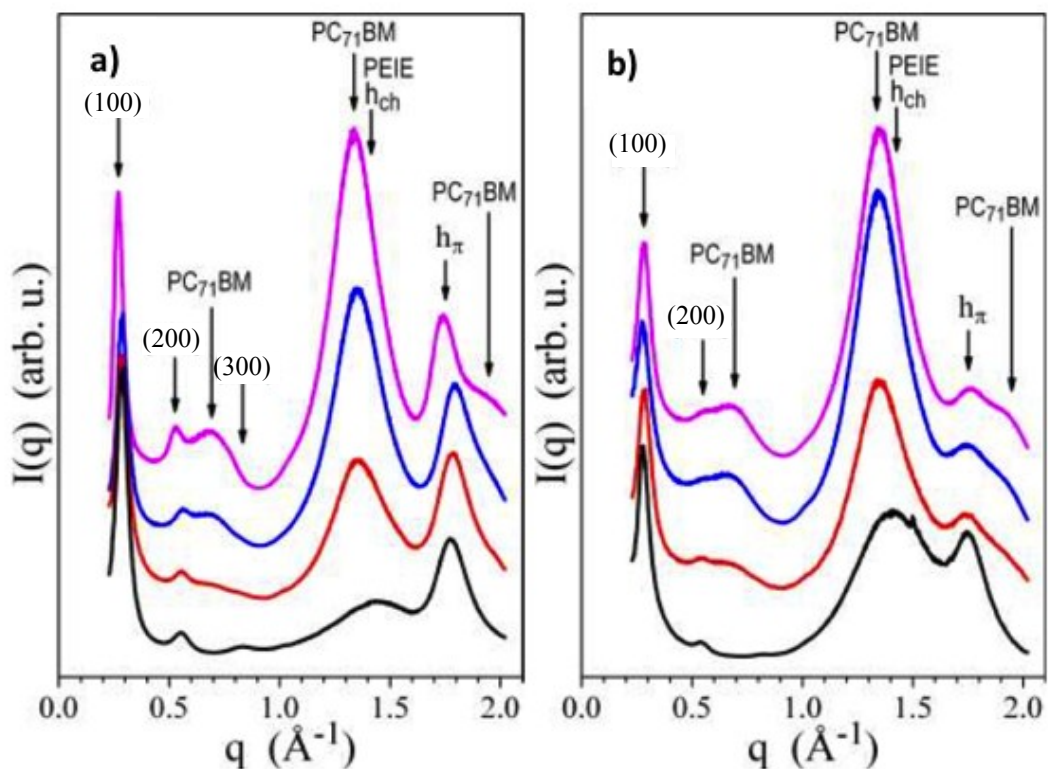


Figure S8: Radial profiles of GIWAXS patterns a) pure PF_2 and $\text{PF}_2:\text{PC}_{71}\text{BM}$ blend films and b) pure PF_0 and $\text{PF}_0:\text{PC}_{71}\text{BM}$ blend films. Pure polymer film (black), polymer:fullerene blend film ratio of 1:1 (red), 1:1.5 (blue) and 1:2 (magenta).

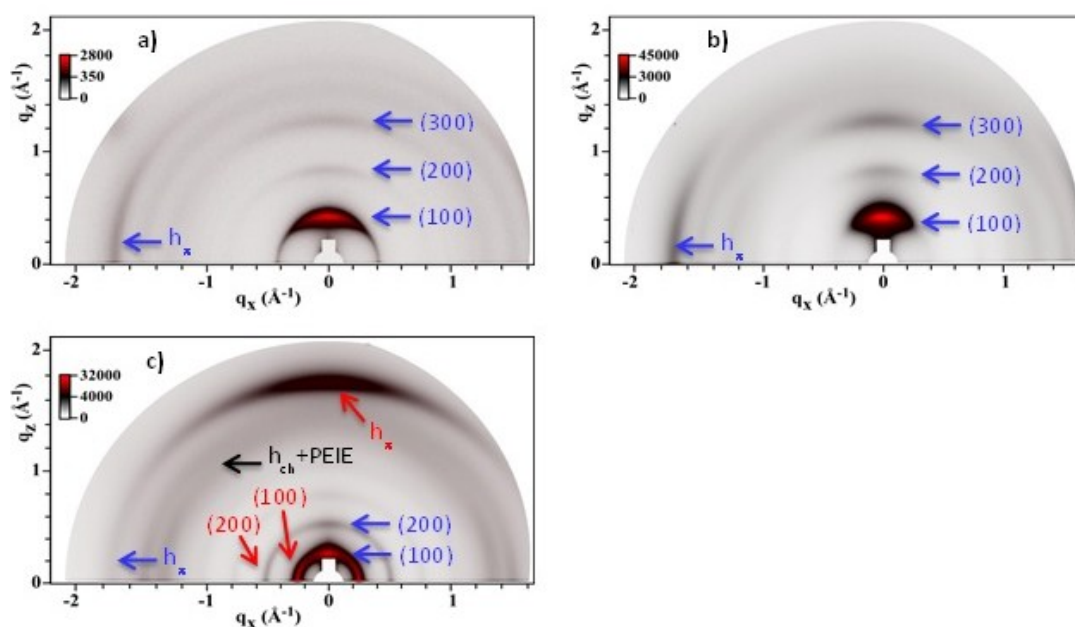


FIGURE S9: GIWAXS patterns of pure a) $\text{PF}_1\text{-T}^+\text{R}_8$; b) $\text{PF}_2\text{-T}^+\text{R}_8$; and c) $\text{PF}_2\text{-T}^+\text{L}_{12}\text{R}_{20}$

6 Scanning Transmission X-ray Microscopy characterizations (STXM).

Scanning Transmission X-ray Microscopy was performed at the STXM instrument (RI GmbH) at HERMES beamline at synchrotron SOLEIL. Thin films (200-300 nm) of $\text{PF}_2:\text{PC}_{71}\text{BM}$, $\text{PF}_0:\text{PC}_{71}\text{BM}$, PF_2 , PF_0 and PC_{71}BM were prepared and floated on to TEM grids for STXM measurements. Horizontally polarized X-rays were incident normal to the sample surface. Sufficient absorption contrast was observed as is evident from the NEXAFS (Near edge x-ray absorption fine structure) spectra of the component films shown in figure 5(e). Energy stacks were obtained at the Carbon K-edge for all the samples. The STXM analysis software aXis2000 (ref: aXis2000 source <http://unicorn.mcmaster.ca/aXis2000.html>), was used for the singular value decomposition (SVD) of the blend stacks using the NEXAFS spectra of the component films.

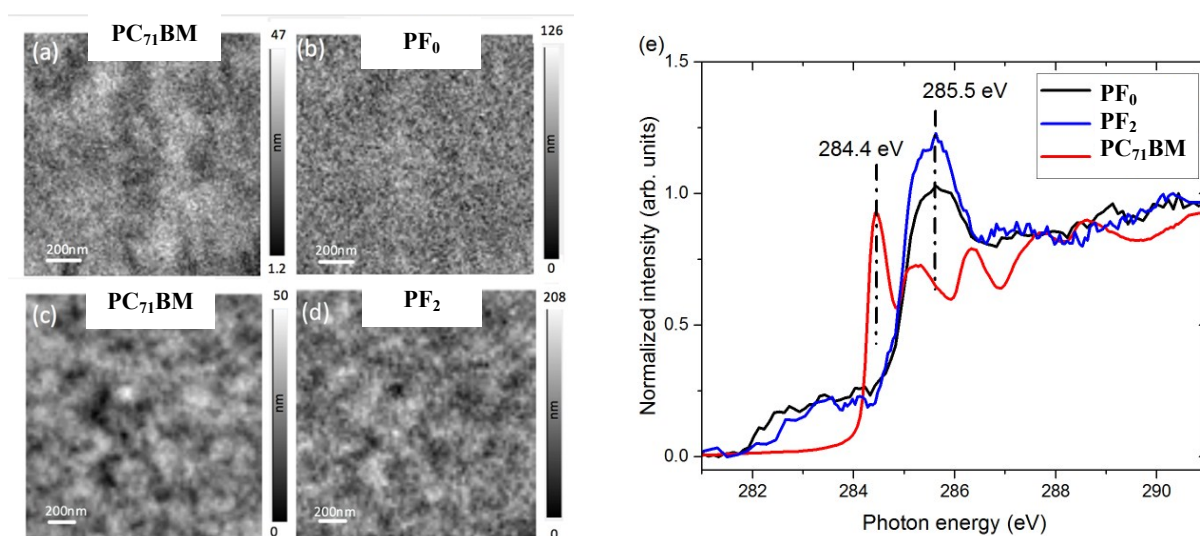


FIGURE S10: Thickness composition maps obtained from STXM energy stacks: (a) PC_{71}BM map and (b) PF_0 map in the $\text{PF}_0:\text{PC}_{71}\text{BM}$ blend, (c) PC_{71}BM map and (d) PF_2 map in the $\text{PF}_2:\text{PC}_{71}\text{BM}$ blend; (e) C K-edge NEXAFS spectra of reference films. The intensity scales represent the calculated thickness in nm's.

7 Fabrication and characterization of solar cells.

ITO coated glass was utilized as a substrate. A thin polyethyleneimine ethoxylated (PEIE) layer (< 10nm) was spin-coated onto pre-cleaned ITO and thermally annealed at 100°C for 10 min and used as an electron extracting electrode. Active layer were elaborated from *o*-DCB solutions using blends of polymers and PC₇₁BM as an electron acceptor material at weight ratio of 1:1.5. The concentrations of solutions for PF₀ and PF₂ based devices were 20 mg/mL and 13 mg/mL with respect to polymer content, respectively. Top electrode consisting of MoO₃ (7 nm)/Ag (120 nm) was thermally evaporated under 5x10⁻⁷ mbar vacuum. Four diodes with a 12 mm² active area were elaborated per substrate. All the characterizations were done in nitrogen atmosphere under dark and simulated AM1.5G irradiation (100 mW/cm², Lot Oriel Sun 3000 solar simulator). The incident light intensity could be changed by the addition of neutral filters.

The device spectral response was measured inside the glove-box using a home-made setup using an Oriel 150 W solar simulator, a Jobin Yvon microHR monochromator (5 nm resolution) and a calibrated Si photodiode fitted after a beam-splitter to measure the incident light power for each wavelength band.

Table S2: Additional photovoltaic parameters for PF₀:PC₇₁BM based devices with standard AM1.5G (100 mW/cm²) illumination.

	Additive	V _{oc} (mV)	J _{sc} (mA/cm ²)	FF (%)	PCE (%)	R _{SH} (Ω)	Thickness (nm)
PF ₀ :PC ₇₁ BM	-	765±10	6.7±0.1	58.6±2	3.01±0.1	5x10 ⁵	140±10
	3% DIO	650±5	8.6±0.2	59.2±1	3.30±0.1	7x10 ⁶	140±10
	-	700±5	5.2±0.5	46.1±1	1.70±0.1	3x10 ⁵	210±10

8 Transient photovoltage and charge extraction measurements.

Transient photovoltage (TPV) and charge extraction (CE) measurements were performed inside the glove box using a home-made set up including a white diode array (Bridgeux; nominal CCT = 5600 K), a green diode and a fast MOS field-effect transistor (MOS-FET).

Discussion on the static and dynamic response of solar cells.

The standard measurements (AM1.5G 100 mW/cm²) on PF₀ and PF₂ solar cells lead to a pronounced difference in photovoltaic performances (PCE lower than 2% for PF₀ and in the 10% range for PF₂). To understand the contributions of the bulky alkyl chains and fluorine atoms to this difference, we investigated the charge carrier dynamics by measuring the solar cell's static and dynamic responses under various illumination conditions. The J_{sc} - light intensity (P_{in}) and $V_{oc} - P_{in}$ curves are given in Figure S11.

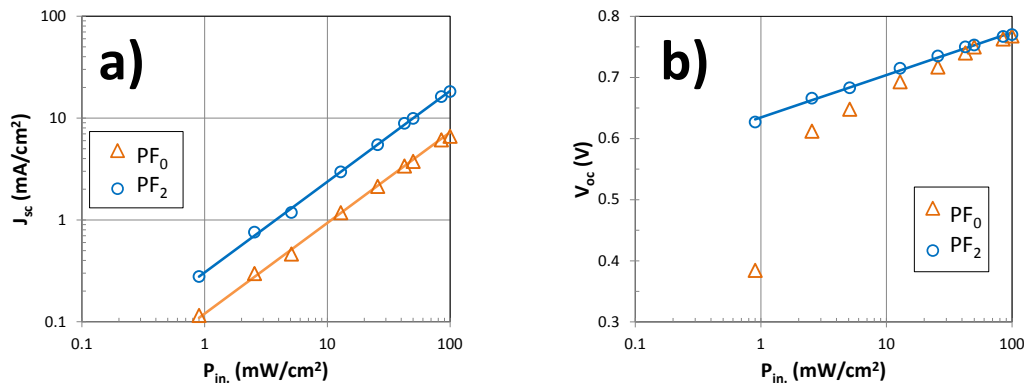


Figure S11: a) J_{sc} as a function of illuminated light power (P_{in}) in log-log scale for both materials. The symbols represent the measurements while the lines correspond to fits using the equation $J_{sc} = J_0(P_{in})^{0.89}$. b) V_{oc} as a function of P_{in} for both copolymers. The symbols represent the measurements while the line corresponds to a fit using equation (1).

The $J_{sc}-P_{in}$ curves follow a power law dependence with a similar exponent (0.89) for both polymers, suggesting a weak contribution of bimolecular recombination in short circuit conditions.^[2] On the other hand, the $V_{oc} - P_{in}$ curves are markedly different for both polymers.

For the fluorinated device, V_{oc} follows:^[3]

$$V_{oc} = a + b \hat{a}^{\text{TM}} \frac{kT}{q} \ln(P_{in}) \quad (1)$$

over the whole investigated intensity range, with T the temperature, q the elementary charge, k the Boltzmann constant and $b = 1.2$. The latter value is close to unity, as expected for bimolecular recombination.^[3] For the non-fluorinated device instead the slope of the curve is steeper at low P_{in} and approaches unity only at the highest light intensity. It is thus likely that trap-limited recombination dominates the charge carrier lifetime in this material at light intensities lower than 10 mW/cm².

To investigate this issue further, transient photo-voltage (TPV) and charge extraction (CE) have been performed on the same devices. In these measurements, the average V_{oc} is fixed by a constant white light source, while a pulsed green light source is used to generate an extra photovoltage (ΔV_{oc}). In the small signal regime, ΔV_{oc} decreases exponentially after each light pulse, with a time constant ($\tau_{\Delta N}$) that equals the charge carrier lifetime at a constant charge carrier density (N).^[4] As the latter increases with the white light source intensity, $\tau_{\Delta N}$ generally follows the equation (See Figure S12a):^[5]

$$\tau_{\Delta N} = \tau_{\Delta N 0} e^{-\hat{V}_{oc}} \quad (2)$$

where the prefactor $\tau_{\Delta N 0}$ represents the charge carrier lifetime at a very low (virtually zero) charge carrier density. In CE measurements, a white light pulse generates the same concentration of free charges as during TPV measurements and those charges are extracted and measured by setting the device in short-circuit conditions. We obtain by CE the following dependence (See Figure S12b):

$$N = N_0 e^{\hat{V}_{oc}} \quad (3)$$

where N_0 is the intrinsic charge-carrier density in the dark.^[4] Combining equations (2) and (3) leads to the dependence of $\tau_{\Delta N}$ as a function of N following equation:

$$\tau_{\Delta N} = \tau_{\Delta N 0} \left(\frac{N_0}{N} \right)^{\hat{V}_{oc}} \quad (4)$$

and shown in Figure S12c. The slope β/γ in equation (4) depends on the main charge-carrier recombination mechanism.^[2]

The experimental $\tau_{\Delta N}(V_{oc})$ curves and fits to equation (2) are shown in Figure S12a and the corresponding values of $\tau_{\Delta N0}$ and β are summarized in Table S3. Interestingly, a single exponential function is observed for the fluorinated device over the whole range of V_{oc} , while a change in the slope occurs at $\approx 0.6V$ for the non-fluorinated device. The latter points towards a change in the recombination mechanism with light intensity, as already highlighted by the stationary response. Note that we observe similar “critical” V_{oc} values for static (Figure S11b) and dynamic measurements (Figure S12b and S12c). The change in slope for the non-fluorinated polymer translates to a change in slope (β/γ) in Figure 12c. The slope at high intensity converges towards the value of the fluorinated device, indicating that under such conditions a similar process is dominating charge recombination. For the fluorinated device, $\tau_{\Delta N}$ is almost proportional to N^{-1} ($\beta/\gamma \approx -1.2$), which would be expected in the case of bimolecular recombination.^[5] On the other hand, for the non-fluorinated device the slope is close to ≈ 0 at low intensity and approaches -1.2 at high intensity. The former value is a distinctive feature of trap-limited recombination and is consistent with the V_{oc} -intensity data discussed above. We may therefore conclude that for PF₀, the recombination mechanism changes from trap-limited to bimolecular recombination when N becomes significantly larger than the trap density. If we further assume that the recombination centers are associated to residual PC₇₁BM molecules in the polymer domains, we may estimate the latter concentration to be at least of the order of 10^{16}cm^{-3} in the non-fluorinated polymer domains.

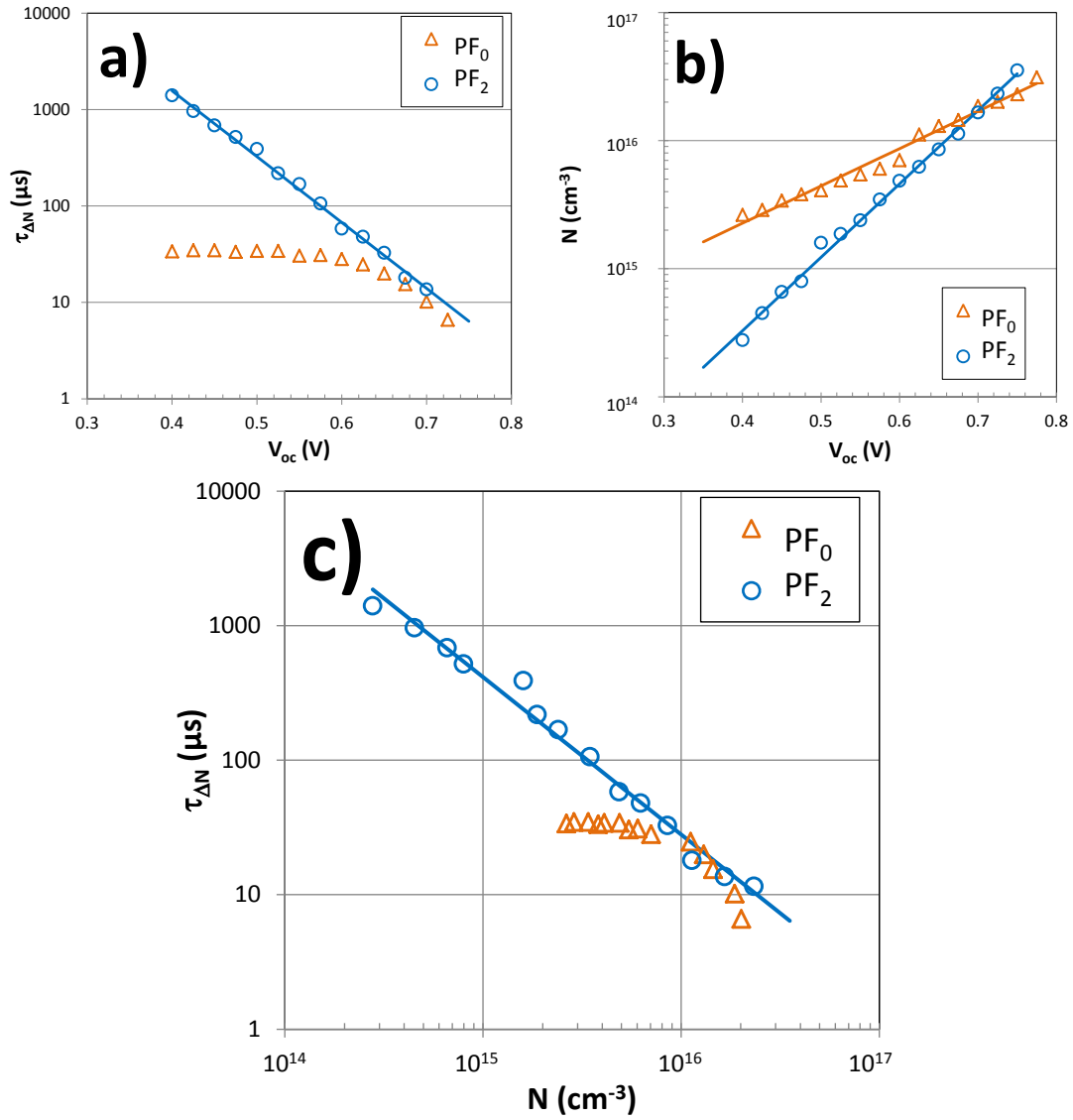


Figure S12: **a)** $\tau_{\Delta N}$ as a function of V_{oc} as measured by TPV (symbols) and fit using Eq. (2) and parameters in Table S3 (line); **b)** N as a function of V_{oc} as measured by CE (symbols) and fit using Eq. (3) and parameters in Table S3 (lines); **c)** $\tau_{\Delta N}$ as a function of N as measured by combining TPV and CE (symbols) and fit using Eq. (4) and parameters in Table S3 (line).

Table S3: fit parameters to TPV and CE data according to Equations (2) to (4).

	$\tau_{\Delta n0}$ (μs)	β (V^{-1})	N_0 (cm^{-3})	γ (V^{-1})	β/γ
PF ₂	9.5×10^5	15.7	1.7×10^{12}	13.2	1.2
PF ₀	-	-	1.5×10^{14}	6.7	-

9 Organic field-effect transistor (OFET) and space-charge limited current (SCLC) devices.

Bottom contact bottom gate OFET structures were fabricated using commercially available silicon substrates. Lithographically defined Au (30 nm)/ITO (10 nm) bilayers were used as source and drain electrodes and 230 nm thick SiO₂ layer as a gate dielectric. Channel length and width were $L = 20 \mu\text{m}$ and $W = 1 \text{ mm}$, respectively. Substrates were cleaned consecutively in ultrasonic baths at 45°C for 15 min each step using soapsuds, acetone, and isopropanol and followed by 15 min UV-ozone treatment. Then substrates were transferred into a nitrogen filled glove box where hexamethyldisilazane (HMDS) was spincoated on top of the SiO₂ followed by annealing at 135°C for 10 min. Finally, pre-heated ($\approx 100^\circ\text{C}$) 5 mg/mL solutions of pure polymers were spincoated on hot ($\approx 100^\circ\text{C}$) substrates to complete the FET devices. Prior to characterization, completed devices were dried under high vacuum ($\approx 10^{-5}$ - 10^{-6} mbar). Transistor output and transfer characteristics were measured using a Keithley 4200 semiconductor characterization system. Hole mobilities were extracted in saturation regime using a standard device model.

Hole-only SCLC diodes were elaborated as follows: ITO coated glass was utilized as a substrate. Cleaning procedure was identical to that of OFET (see above). A thin poly(ethylenedioxythiophene):polystyrene sulfonate (PEDOT:PSS) layer was spincoated onto pre-cleaned ITO and used as a bottom electrode. Polymer and polymer:fullerene layers were spincoated from hot ($\approx 100^\circ\text{C}$) solutions onto pre-heated ($\approx 100^\circ\text{C}$) substrates. Various layer thicknesses were obtained by tuning the solution concentrations. Devices were left overnight under high vacuum ($\approx 5 \times 10^{-7}$ mbar) and were completed by thermally evaporated MoO₃ (7 nm)/Ag (120 nm) layer. SCLC diode (surface area: 0.5 mm²) current-voltage characteristics were measured using a Keithley 4200 semiconductor characterization system.

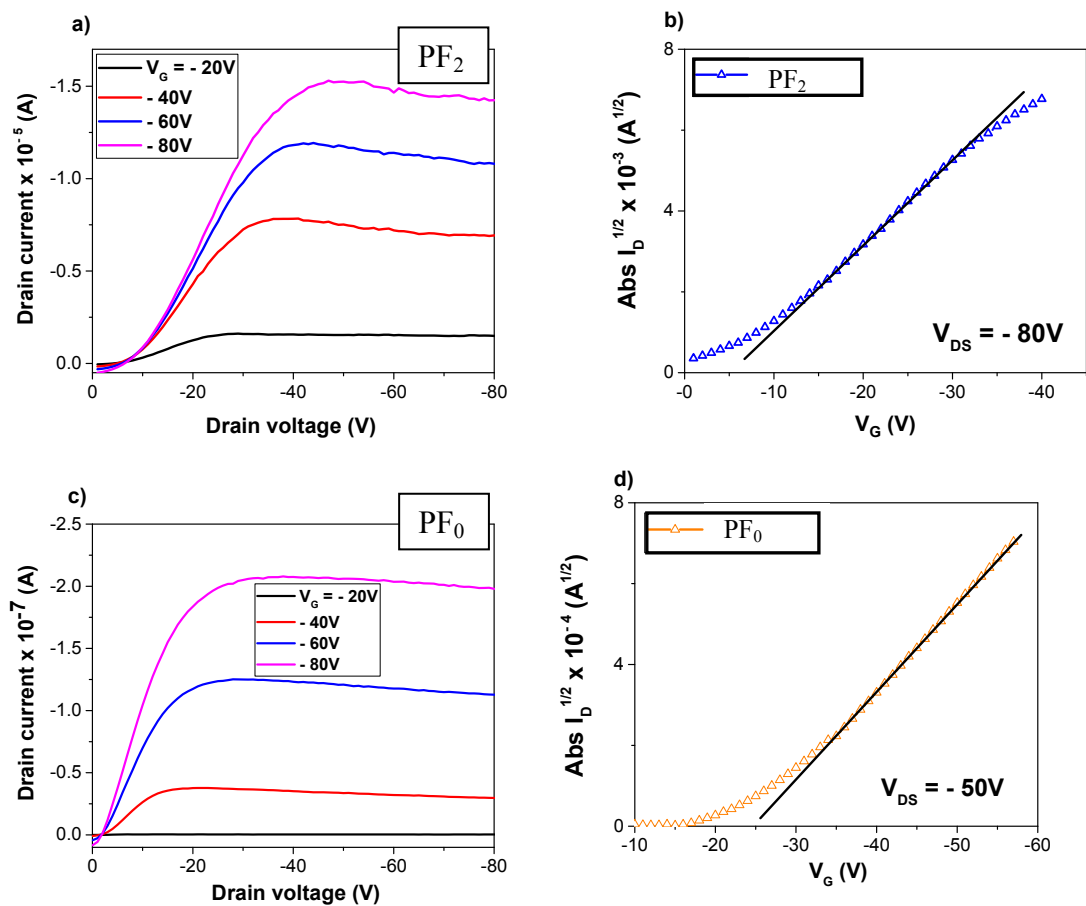


Figure S13: Output (left) and transfer (right) characteristics of OFETs based on pure PF_2 (top) and PF_0 (bottom) copolymers. Solid lines on transfer characteristics represent slopes from which mobility values were extracted.

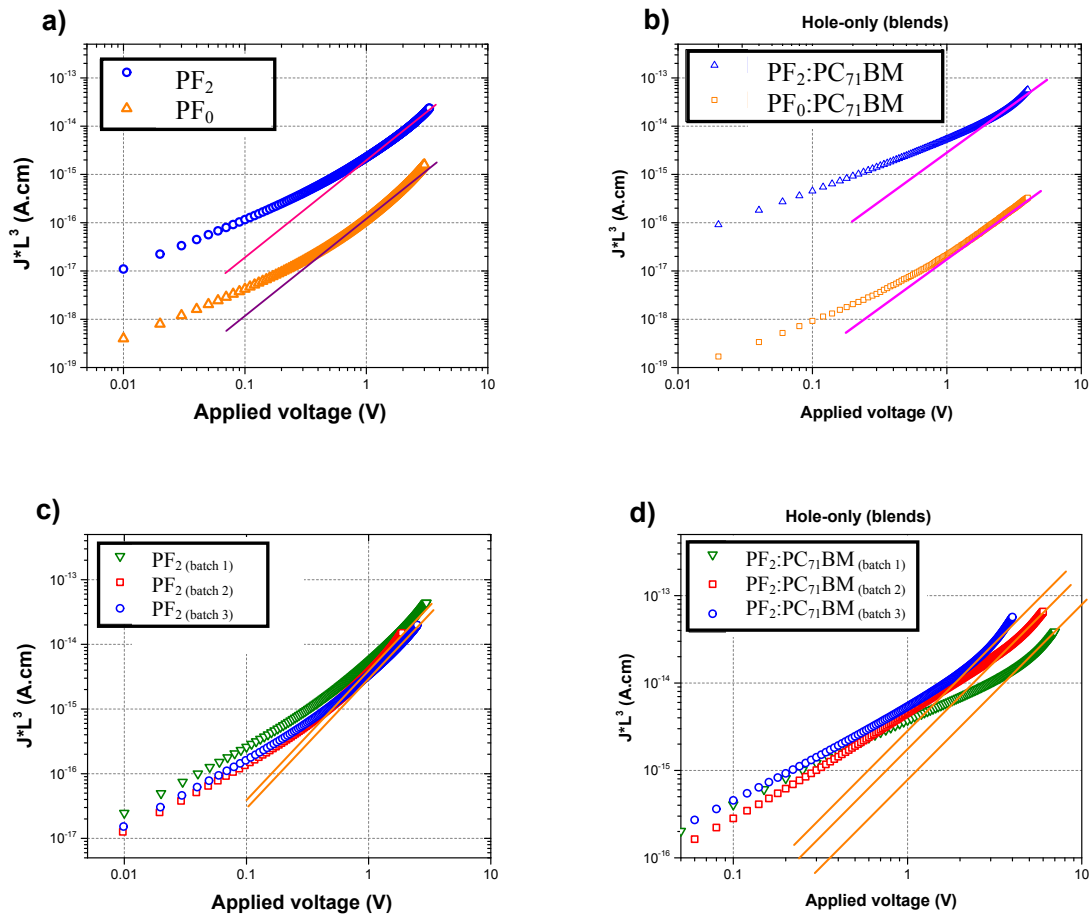


Figure S14: Thickness-scaled current-voltage characteristics of hole-only SCLC devices based on a) pure PF_2 and PF_0 copolymers; b) PF_2 and PF_0 : PC_{71}BM blends c) PF_2 batch x ($x = 1-3$) and d) PF_2 batch x ($x = 1-3$): PC_{71}BM blends. The lines indicate the SCLC regime.

References.

- [1] L. Biniek, S. Fall, C. L. Chochos, D. V. Anokhin, D. A. Ivanov, N. Leclerc, P. Lévêque and T. Heiser, *Macromolecules* **2010**, *43*, 9779.
- [2] C.M. Proctor, M. Kuik, T.-Q. Nguyen, *Prog. Polym. Sci.* **2013**, *38*, 1941.
- [3] A. Chelouche, G. Magnifouet, A. Al Ahmad, N. Leclerc, T. Heiser, P. Lévêque, *J. Appl. Phys.* **2016**, *120*, 225501.
- [4] L.J.A. Koster, V.D. Mihailetschi, R. Ramaker, P.W.M. Blom, *Appl. Phys. Lett.* **2005**, *86*, 123509.
- [5] C.G. Shuttle, B. O'Regan, A.M. Ballantyne, J. Nelson, D.D.C. Bradley, J. de Mello, J.R. Durrant, *Appl. Phys. Lett.* **2008**, *92*, 093311.
- [6] C.G. Shuttle, A. Maurano, R. Hamilton, B. O'Regan, J.C. de Mello, J.R. Durrant, *Appl. Phys. Lett.* **2008**, *93*, 183501.